

# Effects of Many-body Interactions in the Hyperon with Skyrme and KIDS Functionals for Finite Nuclei and Nuclear Matter

Soonchul Choi,<sup>1,2</sup> Emiko Hiyama,<sup>3</sup> Chang Ho Hyun,<sup>4,\*</sup> and Myung-Ki Cheoun<sup>1</sup>

<sup>1</sup>*Department of Physics, Soongsil University, Seoul 06978, Korea*

<sup>2</sup>*Center for Exotic Nuclear Studies,*

*Institute for Basic Science, Daejeon 34126, Korea*

<sup>3</sup>*Department of Physics, Tohoku University, Sendai 980-8578, Japan*

<sup>4</sup>*Department of Physics Education, Daegu University, Gyeongsan 38453, Korea*

(Dated: October 4, 2021)

## Abstract

We investigate  $\Lambda$  hyperon effects on finite  $\Lambda$ -hypernuclei and neutron star matter using an effective nuclear density functional theory, which is based on the chiral effective field theory and has proper multiple density dependence for the effective many-body interactions. Starting from the effective density functional for nucleons, we determine the parameters for the many-body and two-body  $\Lambda$  interactions added to the nucleon energy functional by fitting to some experimental  $\Lambda$ -hypernuclear data. The results turn out to properly explain the data relevant to hypernuclei due to the effective many-body interaction apart from a few data in light hypernuclei. This hyperon functional is exploited to the neutron star.  $\Lambda$  hyperon in the functional shows up in the relatively high density compared to other models including the  $\Lambda$  hyperon. Equation of states and mass radius relations of the hyperonic neutron stars are discussed with the role of the effective interaction for the  $\Lambda$  hyperon beyond the two body interaction.

---

\*Electronic address: hch@daegu.ac.kr

## I. INTRODUCTION

One ultimate goal of hypernuclear physics is to obtain information on baryon-baryon interaction in a unified way. Especially, it becomes important an issue to obtain information on hyperon-nucleon interaction. For this purpose, hyperon( $Y$ )-nucleon( $N$ ) scattering experiment is planned at J-PARC facility. In addition, the study of structure of  $\Lambda$  hypernuclei is essential for obtaining information on  $YN$  interaction. To achieve the goal, there have been intensive efforts by high resolution  $\gamma$ -ray experiments [1, 2]. Then, by combining the data and theoretical calculation such as shell model calculation [3, 4] and few-body calculation [5, 6], we have been obtaining constraints on the spin-independent, spin-spin, and spin-orbit terms of  $\Lambda N$  interaction. As a next stage, it is necessary to study  $\Lambda N - \Sigma N$  coupling, which causes charge symmetry breaking effect in  $\Lambda$  hypernuclei, and effective three-body force. Another important issue is to obtain information on short-range part of effective three-body force, which could contribute to the neutron matter and core of neutron stars. For the study of this three-body force, for instance, M. M. Nagels pointed out that short-range part of  $\Lambda NN$  three-body force gave a contribution to the binding energies of  $\Lambda$  hypernuclei with  $A = 16$  to 208 using recent Nijmegen  $YN$  potential, Extended Soft Core 16 potential model [7]. At J-PARC facility, they plan to perform systematic measurement of energy spectroscopy with wide mass region [8]. Considering this situation, it is required to perform energy spectra of  $\Lambda$  hypernuclei over wide mass region using reliable models and to discuss on the short-range part of  $\Lambda NN$  three-body force.

Along this line, Skyrme force model provides a simple but efficient and robust platform for the access to the problem. In the Skyrme force model, strong forces are approximated to the low energy limit, in which two- and three-nucleon forces could be represented in terms of  $\delta$  functions. Transforming the three-body force to the form of two-body forces, one obtains a term that depends explicitly on density. In the standard Skyrme force, there is only one density-dependent term that is originated from the effective three-body force. It is questionable whether a single density-dependent term would be sufficient for a proper description of the many-body effects. In addition, the original form of the density-dependent term is proportional to density, but in later works the power of the density has been changed to additional numbers (e.g.  $1/3$  or  $1/6$ ) to satisfy certain constraints (e.g. compression modulus or effective mass), or obtain better results from the fitting. In spite of these

ambiguity and arbitrariness, Skyrme force models have been successful in describing the properties of numerous nuclei, from light to heavy, and from the valley of stability to the drip lines. Standard Skyrme force, i.e. a potential with only one density-dependent term has also been applied to  $\Lambda$  hypernuclei [9, 10], and the fitting results in good agreement to the data of single particle levels of the  $\Lambda$  hyperon over a wide range of mass number. However, the issue of arbitrariness in the density-dependent term has not been argued and explored seriously yet.

In the present work, we revisit the interaction of  $\Lambda$  hyperons in nuclear medium at finite density and zero temperature within the framework of nuclear density functional theory. In the KIDS (Korea-IBS-Daegu-SKKU) density functional formalism, similar to the low-energy effective field theory for few-nucleon systems, energy per particle stemming from the strong interaction is expanded in the power of  $k_F/m_\rho$  where  $k_F$  and  $m_\rho$  are the Fermi momentum and rho-meson mass, respectively. At zero temperature  $k_F \propto \rho^{1/3}$  where  $\rho$  is the matter density, so the expansion in terms of  $k_F$  gives rise to multiple density dependence in the in-medium nuclear potential. The expansion rule in the KIDS density functional eliminates the arbitrariness of the density-dependent term in the standard Skyrme force. In addition, the expansion scheme allows one to account for many-body effects beyond the mean field approximation, determine the optimal number of necessary terms to describe finite nuclei and infinite nuclear matter correctly, estimate the uncertainty of theoretical results and predictions, and identify the range of density at which the application of the model is valid. From an extensive analysis, it was shown that the hierarchical priority is established in accordance with the order counting, and the number of terms optimal for both nuclei and nuclear matter is 7 [11, 12]. It's been also shown that with the 7 terms one can obtain correct equation of state (EoS) at densities from the dilute skin of neutrons in neutron-rich nuclei to the center of the most massive neutron stars.

Employing the same expansion rule to the in-medium interaction of  $\Lambda$  hyperons, at first we consider the chi-square of fitting to data as a function of the number of terms in the energy density. If the fitting is saturated at some number of terms, the number may correspond to the optimal number of necessary terms. After the optimal number is fixed, we fit the model parameters to selected  $\Lambda$ -hypernuclear data. Interaction of  $\Lambda$  hyperon in nuclei is certainly affected by the interaction of nucleons. Uncertainties in the interaction of the nucleon will be imperatively propagated to the interaction of  $\Lambda$  hyperons. We consider the uncertainty

in the density dependence of the nuclear symmetry energy, and several sets of parameters for the interaction of  $\Lambda$  hyperons are obtained as a result. After the model parameters are determined, we apply the models of  $\Lambda$  hyperon to the prediction of properties of hypernuclei whose data are available but not used in the fitting. Next to the finite nuclei, we consider the neutron star. Creation of the hyperon within the neutron star core is critically sensitive to the stiffness of the symmetry energy. Most concerned issue might be the role of hyperons to the radius of neutron stars of mass  $(1.0-2.0)M_\odot$ . Our result will shed light on understanding relevance or irrelevance of hyperons to the existing and coming up neutron star data.

## II. FORMALISM

In the KIDS formalism, energy density functional is expanded in powers of Fermi momentum, or equivalently  $\rho^{1/3}$  where  $\rho$  is the baryon density. Functionals for the nucleon are described and explained in detail in the previous publications (see e.g. [12]). For the many-body interactions of  $\Lambda$  hyperons such as  $\Lambda NN$ , we assume a similar expansion in terms of the nucleon density as

$$H_{\Lambda\rho} = \frac{3}{8}\rho_\Lambda \sum_{i=1}^{N_f} u_{3i} \left(1 + \frac{1}{2}y_{3i}\right) \rho_N^{1+i/3}. \quad (1)$$

This new type of functional is added to the two-body interaction terms given as

$$\begin{aligned} H_{\Lambda N} = & \frac{\hbar^2}{2m_\Lambda} \tau_\Lambda + u_0 \left(1 + \frac{1}{2}y_0\right) \rho_N \rho_\Lambda \\ & + \frac{1}{4}(u_1 + u_2)(\tau_\Lambda \rho_N + \tau_N \rho_\Lambda) + \frac{1}{8}(3u_1 - u_2)(\nabla \rho_N \cdot \nabla \rho_\Lambda) \\ & + \frac{1}{2}W_\Lambda(\nabla \rho_N \cdot \vec{J}_\Lambda + \nabla \rho_\Lambda \cdot \vec{J}_N). \end{aligned} \quad (2)$$

Model parameters  $u_0$ ,  $y_0$ ,  $u_1$ ,  $u_2$ ,  $W_\Lambda$ ,  $u_{3i}$  and  $y_{3i}$  are fitted to  $\Lambda$ -hypernuclear data.  $\Lambda$ -hypernuclear data are available over wide range of mass number from He to Pb. Since the mean field approximation is justified to work well in the large mass number systems, we consider the data of masses above Oxygen. In Tab. I, we summarize the  $\Lambda$ -hypernuclear data that are used in fitting the model parameters. Data for higher orbitals such as  $f$  and  $g$  are available, but in order to examine the predictive power of the theory, they as well as the data of light nuclei will be compared with the prediction of the theory.

In the KIDS formalism, higher order contributions are added systematically, so it is adjustable to find the number of terms that reproduce the nuclear data optimally. In order

Nuclei	$1s$ (MeV)	$1p$ (MeV)	$1d$ (MeV)
$^{16}_{\Lambda}\text{O}$ [13, 14]	$12.50 \pm 0.35$		
$^{28}_{\Lambda}\text{Si}$ [2, 15]	$16.60 \pm 0.20$	$7.0 \pm 0.2$	
$^{32}_{\Lambda}\text{S}$ [16]	$17.50 \pm 0.50$		
$^{40}_{\Lambda}\text{Ca}$ [17, 18]	$18.70 \pm 1.1$		
$^{51}_{\Lambda}\text{V}$ [19, 20]	$19.9 \pm 1.0$		
$^{89}_{\Lambda}\text{Y}$ [2, 20]	$23.10 \pm 0.50$	$16.50 \pm 4.1$	$9.1 \pm 1.3$
$^{139}_{\Lambda}\text{La}$ [2]	$24.50 \pm 1.20$	$20.40 \pm 0.6$	$14.3 \pm 0.6$
$^{208}_{\Lambda}\text{Pb}$ [2]	$26.30 \pm 0.80$	$21.90 \pm 0.6$	$16.8 \pm 0.7$

TABLE I: Experimental data of the single particle levels of a  $\Lambda$  hyperon in nuclei used in determining the in-medium interaction of a  $\Lambda$  hyperon given by Eqs. (1,2).

to find the optimal number of terms for the interaction of the  $\Lambda$  hyperon in nuclear medium, we consider the number of terms  $N_f$  in Eq. (1) from 1 to 5. Each model labeled with  $YN_f$  is fitted to data in Tab. I, and the accuracy is measured by  $\chi^2$  defined as

$$\chi^2 = \frac{1}{N_d} \sum_{i=1}^{N_d} \left( \frac{M_i^{\text{exp}} - M_i^{\text{cal}}}{\sigma_i} \right)^2. \quad (3)$$

Figure 1 shows the result of fitting together with the data adopted in the fitting.  $\chi^2$  value is denoted in the parentheses at the end of legend for  $YN_f$ . As it has to be, accuracy of the model is improved as the number of terms is increased, but rather than a monotonic behavior,  $\chi^2$  decreases step-wisely. Improvement from Y1 to Y2 is dramatic, and Y2 and Y3 reproduce the input data at a similar accuracy. Agreement to data is more improved in Y4, and there is a small difference between Y4 and Y5. In the Y1 model, fitting result does not come in the experimental error bars at 5 data points:  $^{16}\text{O}$ ,  $^{28}\text{Si}$ ,  $^{208}\text{Pb}$  in the  $1s$  state,  $^{208}\text{Pb}$  in the  $1p$  state, and  $^{89}\text{Y}$  in the  $1d$  state. A similar mismatch of the fitting result and data is obtained in Ref. [9] where only a single  $\Lambda\rho$  interaction is considered. On the other hand, the models having multiple  $\Lambda\rho$  interactions Y2 – Y5 give all the results within the experimental uncertainty ranges.

It is natural to guess that if more high order terms are added,  $\chi^2$  value could be reduced furthermore. However, in the consideration of nucleon, we learned that the optimal number of terms for accurate description of the nuclear matter EoS up to densities at the center of

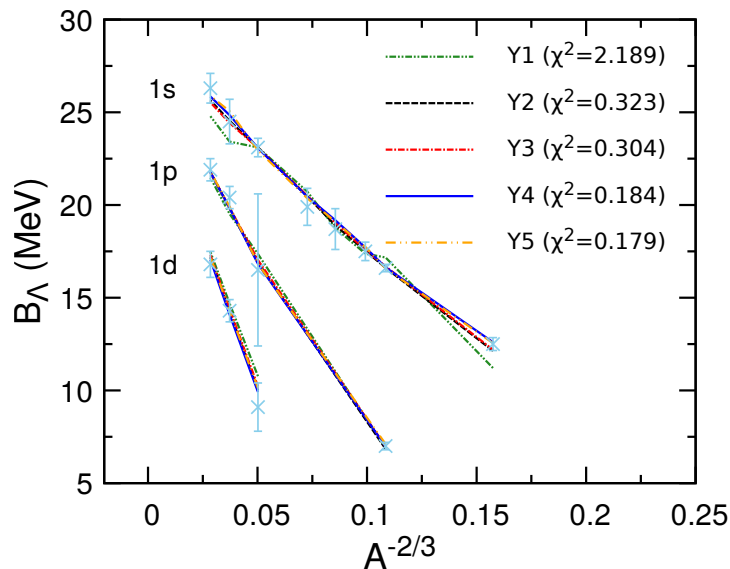


FIG. 1: Result of fitting to the data in Tab. I with the KIDS0 model and the number of  $\Lambda\rho$  interaction terms from 1 to 5.

the most massive neutron star is 3 (symmetric matter) or 4 (neutron matter) [11, 12]. We expect that this will also be the case for the  $\Lambda$  hyperon, and 4 terms will suffice for the reliable description of hypernuclear matter EoS up to the density in the neutron star core. In the application of the model afterwards, we will consider only the 4-term model (Y4) for the interaction of  $\Lambda$  hyperon.

Density dependence of the nuclear symmetry energy is an essential issue because experiments that are most directly concerned to the issue report interesting results from measurements and observations recently. Density dependence of the symmetry energy is conventionally expanded around the saturation density  $\rho_0$  as

$$S(\rho) = J + Lx + \frac{1}{2}K_{\text{sym}}x^2 + \dots, \quad (4)$$

where  $x = (\rho - \rho_0)/3\rho_0$ . Behavior around  $\rho_0$  is most sensitive to the value of  $L$ , and then  $K_{\text{sym}}$ . These parameters are critical in determining the structure of neutron rich nuclei, and bulk properties of the neutron star, but uncertainty is still large. In a recent work, several sets of symmetry energy parameters  $J$ ,  $L$ ,  $K_{\text{sym}}$  have been derived, which satisfy both nuclear data and neutron star observation [21]. Four models labeled KIDS-A, B, C, D in [21] have different values of  $J$ ,  $L$ , and  $K_{\text{sym}}$  as well as the compression modulus  $K_0$ ,

	KIDS0	KIDS-A	KIDS-B	KIDS-C	KIDS-D
$K_0$	240	230	240	250	260
$J$	32.8	33	32	31	30
$L$	49.1	66	58	58	47
$K_{\text{sym}}$	-156.7	-139.5	-162.1	-91.5	-134.5

TABLE II: Nuclear matter properties at the saturation density for KIDS models. All the models have identical saturation density  $0.16 \text{ fm}^{-3}$  and the binding energy per nucleon 16 MeV. Compression modulus  $K_0$ , and the symmetry energy parameters  $J$ ,  $L$ , and  $K_{\text{sym}}$  are in the unit of MeV.

so they provide a good test ground to explore the effect of uncertainties in symmetric and asymmetric nuclear matter to the in-medium interaction of  $\Lambda$  hyperons, and consequent properties of the neutron star. It has been shown that the creation of  $\Lambda$  hyperons in the core of a neutron star, and consequential bulk properties of neutron stars depend strongly on the EoS of nucleonic matter which is the background on which hyperons are created [22]. Compression modulus and the symmetry energy coefficients of the models are compared in Tab. II.

### III. MANY-BODY EFFECTS ON THE NUCLEON AND HYPERON PARTS

#### A. For Finite Nuclei

For a consistent determination of the  $\Lambda$  hyperon interaction, parameters in the Y4 interaction have to be fitted to the data in Tab. I for each model. Results for the parameters and the  $\chi^2$  are summarized in Tab. III. As a whole parameters are similar to each other, but a few sizable differences also exist. Magnitude of  $u_{31}$  differs by a factor of 2. Negative sign implies attractive force. It means that if a coefficient in the potential energy is negative and large in magnitude, it makes the chemical potential of  $\Lambda$  hyperon small, and it leads to early onset of the hyperon creation, which subsequently makes the equation of state soft.

In order to understand the behavior of  $\Lambda$  hyperon potential more precisely, we consider the Hamiltonian density given by Eq. (1) and the term proportional to  $u_0$  in Eq. (2) divided

	KIDS0	KIDS-A	KIDS-B	KIDS-C	KIDS-D
$u_0$	-160.95264	-128.81502	-169.22118	-125.07505	-125.94104
$u_1$	70.76000	94.95210	56.69966	85.71671	75.82594
$u_2$	-15.02857	-5.14575	-12.34702	-7.23919	-11.74793
$u_{31}$	-422.21514	-398.48003	-371.23408	-231.60546	-206.39651
$u_{32}$	373.02533	265.47960	222.62548	276.26060	359.13476
$u_{33}$	248.20334	276.00074	220.71935	208.07528	190.90642
$u_{34}$	-304.90644	-298.23538	-114.46241	-299.70071	-270.48269
$y_0$	3.95994	5.19600	3.67720	5.75962	5.33203
$y_{31}$	-6.60578	-7.65872	-8.29438	-9.53907	-8.17689
$y_{32}$	5.65621	-1.45742	9.06089	7.47400	9.44507
$y_{33}$	-0.89714	6.40191	-2.14865	7.10293	-4.59458
$y_{34}$	-2.15451	-5.52651	-4.17324	2.09727	-0.53146
$\chi^2$	0.1844	0.2096	0.2229	0.2085	0.2093

TABLE III: Model parameters obtained from fitting to the data in Tab. I. Units are MeV fm<sup>3</sup> for  $u_0$ , MeV fm<sup>5</sup> for  $u_1$  and  $u_2$ , and MeV fm<sup>3+i</sup> for  $u_{3i}$ .  $y_0$  and  $y_{3i}$  are dimensionless.

by  $\rho_\Lambda$ ;

$$\begin{aligned}
h_3(\rho_N) &= \frac{H_{\Lambda\rho}}{\rho_\Lambda} = \frac{3}{8} \sum_{i=1}^N u_{3i} \left(1 + \frac{1}{2} y_{3i}\right) \rho_N^{1+i/3}, \\
h_0(\rho_N) &= u_0 \left(1 + \frac{1}{2} y_0\right) \rho_N.
\end{aligned} \tag{5}$$

Since  $u_1$  and  $u_2$  are smaller than  $u_0$  and  $u_{3i}$  by orders of magnitude, we omit those terms in the consideration.

Figure 2 presents the result. Two-body contribution  $h_0$  is similar, and actual difference originates from the many-body terms in  $h_3$ . Sum of  $h_0$  and  $h_3$  shows non-negligible model dependence. The behavior in  $\rho_N = 0.3 - 0.5 \text{ fm}^{-3}$  is especially notable because many models predict that hyperons begin to exist in the core of neutron stars in this density range. Calculation of the neutron star will reveal the sensitivity to the softness or stiffness of the  $\Lambda$  hyperon interaction.

At densities above  $0.5 \text{ fm}^{-3}$ , models again show clear difference. KIDS-A model increases



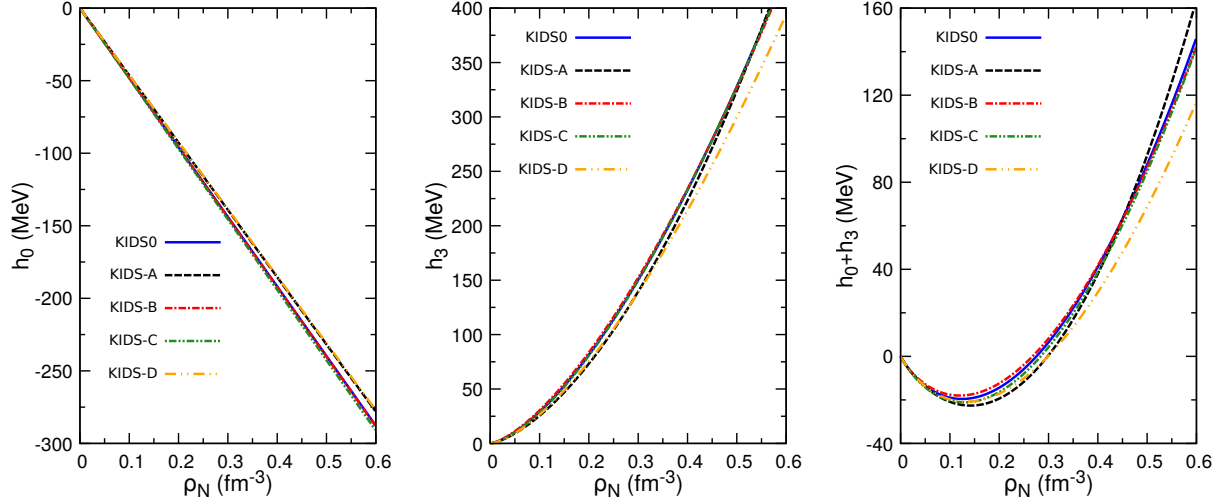


FIG. 2:  $h_0$  (left),  $h_3$  (center) defined in Eq. (5), and  $h_0 + h_3$  (right) as functions of the nucleon density  $\rho_N$ .

fastest, KIDS0, B, C models are similar, and KIDS-D model is by far softer than other models. Softness of the KIDS-D model could be understood from the sign of  $u_{33}$  term: sign of the term in the KIDS-D model is negative, but it is positive in the other models. Stiffness at this high density could have significant effect on the particle fraction in the neutron star core, which affects the stiffness of EoS, and consequently the mass-radius relation and the maximum mass. Results for the neutron stars will be discussed in the following subsection.

Prior to the consideration of neutron stars, we first examine the performance of models in nuclei. Results are summarized in Fig. 3. Lines denote the theoretical result, and empty green triangles represent the data used in the fitting. Data unemployeed in the fitting consist of the levels of nuclei lighter than  $^{16}\text{O}$  [23–29], and the levels in the  $f$ - and  $g$ -orbitals in heavy nuclei [2, 20]. They are marked in filled red circles. Theory lines overlap so closely that it is not necessary to distinguish models when nuclear properties are referred to. This coincidence could be understood from the similarity of  $\chi^2$  values in Tab. III.

Without exception, theory reproduces the input data within the error bars. In the  $1f$  and  $1g$  states, model prediction is also within the experimental uncertainties. However, comparison with the levels in the light nuclei is not as good as heavy nuclei. Models consistently underestimate the experimental data. Fitting with light nuclei as well as heavy ones was performed in [9, 10]. When the light nuclei data are accounted in the fitting, result of theory

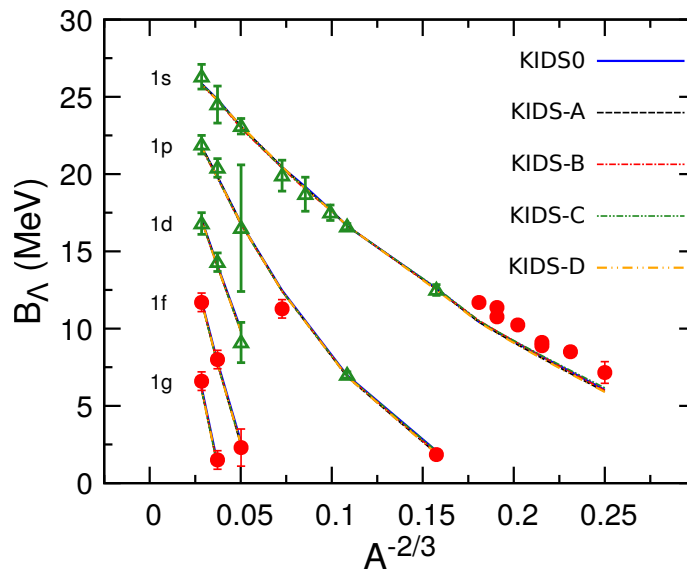


FIG. 3: Single particle levels for the KIDS-0, KIDS-A, KIDS-B, KIDS-C and KIDS-D models with Y4 hyperon interaction and from data.

for the light nuclei becomes better than this work. In that case, however, theory does not reproduce a few data for heavy nuclei. For example, HPA2 model in [9] gives a result out of the data of  $1s$  state in  $^{208}\text{Pb}$ . There is a mismatch with data of  $^{28}\text{Si}$  in the  $1s$  state [10]. Since we focus on the predictive power of theory in the intermediate and large mass number region, the agreement in the  $1f$  and  $1g$  states is thought to be enough for the remained process. Problem in light nuclei could be explored in detail in a separate work.

## B. For Nuclear Matter

$\Lambda$  hyperons embedded in hypernuclei are surrounded by nucleons at densities close to the nuclear saturation. Therefore, hypernuclear data is likely to suggest constraints relevant to the  $\Lambda$  hyperon interactions at the saturation density. Models thus determined are expected to describe well the hypernuclear phenomenology at the saturation density, and in addition applicable to densities below or above the saturation density to a certain extent. Neutron star provides an ideal laboratory for probing the validity of hypernuclear models at densities well above the saturation density. The application to neutron star is especially important for finding a solution to the hyperon puzzle problem in the neutron star.

Equation of state of the matter in the core of neutron stars is obtained as a function of the particle density. Density of each particle is obtained as solutions of the charge neutrality

$$\rho_p = \rho_e + \rho_\mu, \quad (6)$$

and chemical equilibrium

$$\mu_n = \mu_p + \mu_e + \mu_\mu = \mu_\Lambda, \quad (7)$$

where  $\mu_i$  denotes the chemical potential of particle  $i$ .

Figure 4 shows the particle fraction defined as  $\rho_i/\rho_B$  where  $\rho_i$  is the density of particle  $i$  and  $\rho_B = \rho_n + \rho_p + \rho_\Lambda$  is the total baryon density. SLy4+HPA2 model in Ref. [9] is included for comparison. The density  $\rho_{\text{crit}}$  at which  $\Lambda$  starts to build up varies significantly. In the unit of saturation density,  $\rho_{\text{crit}}$  are obtained as 2.8, 4.4 3.5, 3.3 and 3.2 for SLy4, KIDS0, KIDS-B, KIDS-C and KIDS-D, respectively. In the majority of models considering hyperons in the neutron star,  $\rho_{\text{crit}}$  is located in the range  $(2-3)\rho_0$  [22], but the KIDS models consistently obtain  $\rho_{\text{crit}}$  larger than  $3\rho_0$ . Even no hyperon creation is predicted in the KIDS-A model. In Ref. [30], two-body  $\Lambda N$  and three-body  $\Lambda NN$  forces are calculated with chiral effective field theory (EFT), and the result is applied to the creation of  $\Lambda$  hyperons in the core of the neutron star. Conclusion is that  $\Lambda$  is not created in the neutron star. Looking into the behavior of chemical potentials, chiral EFT obtains the result very similar to that of KIDS-A model. Details will be discussed when the chemical potential is considered.

Production rate of  $\Lambda$  also depends on the model. The standard SLy4 model shows relatively slow increase of the number of  $\Lambda$  hyperon compared to the KIDS model. Among the KIDS models, B, C, D models show similar behavior, but the populaion of  $\Lambda$  increases explosively right after it is created in the KIDS0 model. The different results in the particle fraction such as  $\rho_{\text{crit}}$  and production ratio can be understood well in terms of the chemical potential.

Figure 5 shows the chemical potential of the neutron and  $\Lambda$  hyperon in the core of a neutron star as functions of density. All the models show  $\mu_n$  increases monotonically before the chemical equilibrium condition is satisfied.  $\mu_\Lambda$  is in decreasing phase up to  $0.2 \text{ fm}^{-3}$  in the SLy4+HPA2 model, but the KIDS models show decreasing behavior up to about  $0.1 \text{ fm}^{-3}$ , and change to increasing phase afterwards. Hyperon creation density  $\rho_{\text{crit}}$  becomes small when  $\mu_n$  increases fast or  $\mu_\Lambda$  increases slowly. Early creation of  $\Lambda$  hyperons in the SLy4+HPA2 model is mainly originated from slow increase of  $\mu_\Lambda$  relative to the KIDS

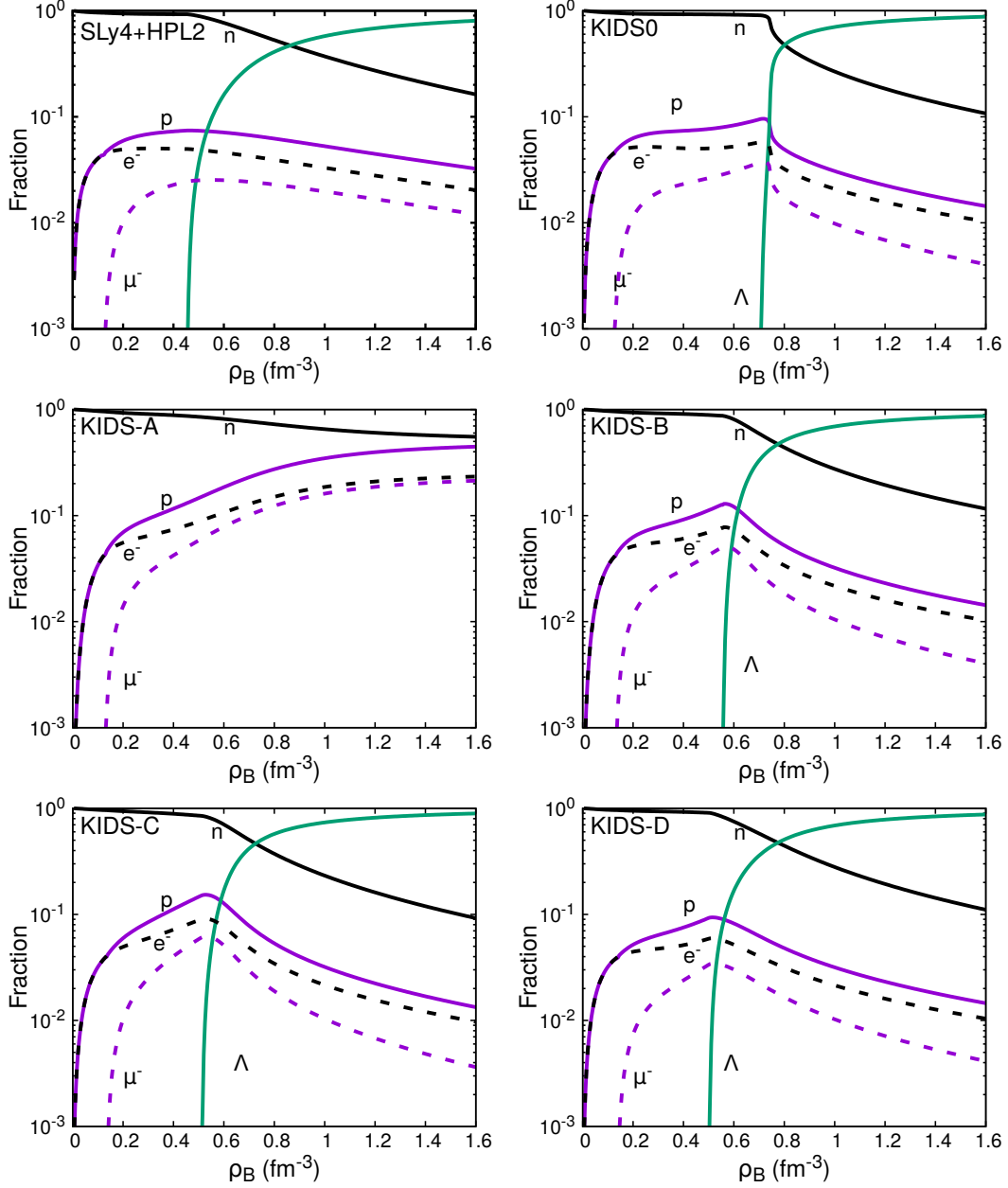


FIG. 4: Particle fraction in the core of neutron stars as a function of density for the SLy4+HPA2, KIDS0, KIDS-A, KIDS-B, KIDS-C and KIDS-D models with Y4 hyperon interaction.

models. Large  $\rho_{\text{crit}}$  in the KIDS0 model, on the other hand, is because of the slow increase of  $\mu_n$  compared to other KIDS models. For example, at  $\rho = 0.6 \text{ fm}^{-3}$ ,  $\mu_n$  in the KIDS0 model is about 1250 MeV, but it is about 1300 MeV in the KIDS-A model.

Equation of state of nucleonic matter of the SLy4 model is very similar to that of the KIDS0 model, so the comparison of the two models exhibits most clearly the difference

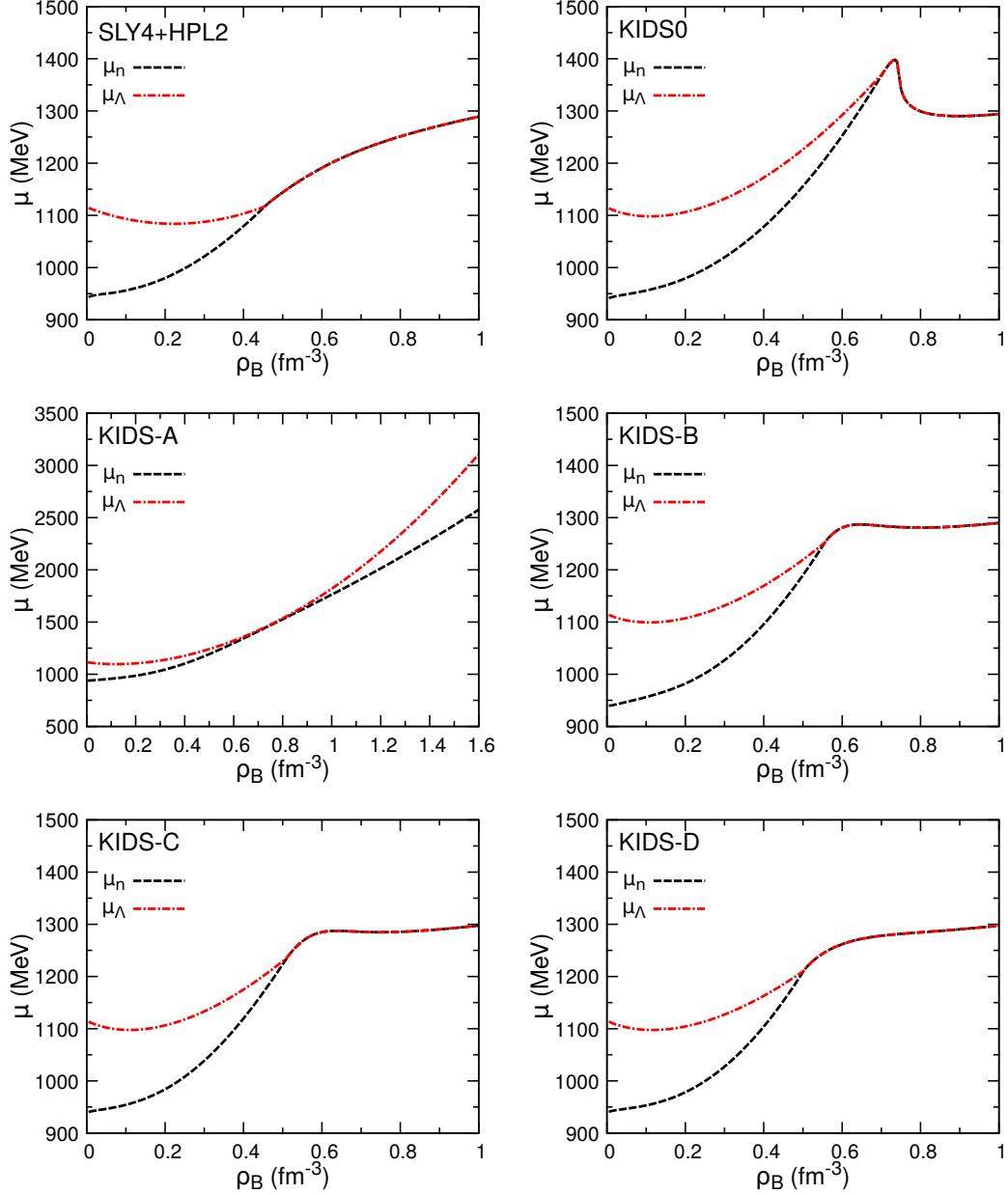


FIG. 5: Chemical potentials of the neutron and the  $\Lambda$  hyperon for each model.

arising from hyperons. In the KIDS-Y4 models,  $\mu_\Lambda$  is increasing faster than the HPA2 model. This difference makes huge difference in  $\rho_{\text{crit}}$  between SLy4+HPA2 and KIDS0-Y4. Fast increase of  $\mu_\Lambda$  in the Y4 models is mainly due to the contribution from the higher order terms in the multiple density-dependent description of interactions. Contribution of the multiple density dependence is essential in reproducing the hypernuclear data accurately and obtaining stability in the fitting, but also critical in approaching to a complete description

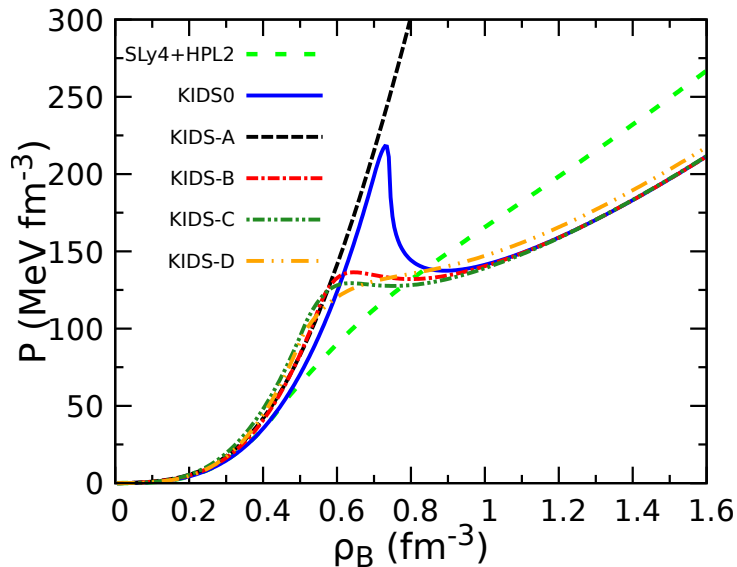


FIG. 6: Pressure as a function of density for the KIDS0, KIDS-A, KIDS-B, KIDS-C and KIDS-D models with Y4 hyperon interaction. Result of the SLy4+HPA2 model is compared.

of neutron star EoS at supra densities.

The result of KIDS-A model is shown in scales of  $x$  and  $y$  axes larger than other models to make sure the non-existence of  $\Lambda$  hyperon. At densities  $\rho \leq 2\rho_0$ ,  $\mu_n$  is substantially smaller than  $\mu_\Lambda$ . As the density passes through  $2\rho_0$ ,  $\mu_n$  approaches to  $\mu_\Lambda$  quickly, and the two chemical potentials move very closely from  $3\rho_0$  to  $6\rho_0$ . Above  $6\rho_0$ , increase rate of  $\mu_\Lambda$  overwhelms that of  $\mu_n$ , so there is no chance for  $\Lambda$  hyperon to inhabit in the neutron star. The overall behavior such as substantial difference below  $2\rho_0$ , and similar values in  $(3-5)\rho_0$  resembles the result of chiral EFT [30].

$\mu_n$  of KIDS-B and D models behave similarly at  $\rho \leq 5\rho_0$ , and  $\mu_n$  of KIDS-C model is slightly stiffer than B and D models. On the other hand,  $\mu_\Lambda$  of KIDS-B and C models increases at similar rate before  $\Lambda$  hyperon is created, and  $\mu_\Lambda$  of KIDS-D model is softer than the B and C models.  $\rho_{\text{crit}}$  is lowered when  $\mu_n$  is stiff or  $\mu_\Lambda$  is soft. Since  $\mu_n(\text{KIDS-C}) > \mu_n(\text{KIDS-B})$ , and  $\mu_\Lambda(\text{KIDS-D}) < \mu_\Lambda(\text{KIDS-B})$ ,  $\Lambda$  hyperons are created at densities smaller than the KIDS-B model in the KIDS-C and D models. In a nutshell, KIDS-Y4 models illustrate the high threshold energy compared to other models including hyperons.

A star could be in stable state when inward gravitation is balanced with outward repulsion. In the neutron star, repulsive force from the strong interaction takes the role of

balance with gravitation. A key quantity is the pressure which is the gradient of energy density along the radial direction. Figure 6 shows the pressure as a function of density.

Similarity of SLy4 and KIDS0 could be seen from the pressure. Pressure of the two models is almost identical up to  $\rho = 0.45 \text{ fm}^{-3}$  where  $\Lambda$  is created in the SLy4+HPA2 model. Huge difference since then is totally attributed to the difference in the  $\Lambda$ -hyperon interactions. The result confirms the importance of correct description of  $\Lambda$ -hyperon interactions at high densities. Since  $\Lambda$  hyperon is absent in the KIDS-A model, the result shows the behavior pure nucleonic matter EoS.

In the SLy4+HPA2 model, transition from nucleonic matter to the strangeness-mixed phase happens smoothly, so the pressure changes smoothly at densities hyperons are created. In contrast, KIDS models show abrupt bending down of the pressure, and there is an unstable region where  $dP/d\rho < 0$ . Occurrence of the unstable region in the KIDS model could be understood from the particle fraction. Relative to the SLy4+HPA2 model,  $\Lambda$  is created very rapidly in the KIDS model, especially KIDS0. Abrupt and numerous creation of  $\Lambda$  relieves the strong degeneracy compiled by the neutron, and this leads to instantaneous collapse of the pressure. These unstable regions, if they exist within a star, will collapse and disappear from the star, so that  $dP/d\rho \geq 0$  will be satisfied in the whole interior of the star. Maxwell or Gibbs constructions are conventionally used when EoS is supposed to be obtained without unstable region.

Comparison of KIDS-A with other models show how much the EoS is softened by the existence of hyperonic matter. Pressure is reduced dramatically. The effect will affect the upper limit of density up to which strong interaction can make balance with gravitation, and thus the mass range permitted to stable neutron stars. Figure 7 shows the mass and radius (MR) relation of neutron stars. If only the nucleons are considered, all the models have maximum masses larger than  $2M_{\odot}$ . KIDS-A model shows traditional behavior of stars composed of nucleons only, and the difference from the KIDS-A model is originated from the  $\Lambda$  hyperons in the star.

If hyperon is not considered, the SLy4 model shows MR relation very similar to that of the KIDS0 model [31]. In the SLy4+HPA2 model,  $\Lambda$  hyperons starts to be created in the star of mass  $\sim 1.2M_{\odot}$  [22], and the mass reaches maximum at  $\sim 1.5M_{\odot}$ . In the KIDS0 model, MR curve rises up smoothly and encounters a sharp change at  $M \sim 1.9M_{\odot}$ . Abrupt change of the MR curve is caused by the creation of the  $\Lambda$  hyperon. Mass of the star where

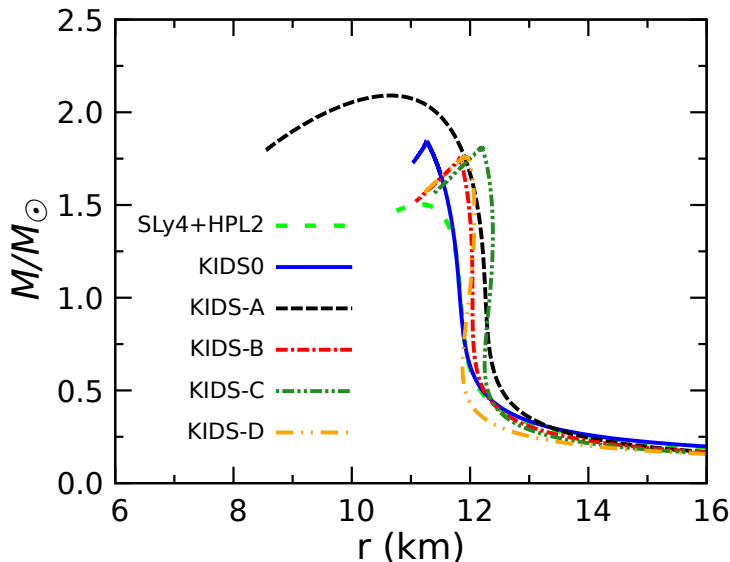


FIG. 7: Mass-radius relation of neutron stars for the KIDS0, KIDS-A, KIDS-B, KIDS-C and KIDS-D models with Y4 hyperon interactions. Result of the SLy4+HPA2 model is compared.

$\Lambda$  is created ( $M_{\text{crit}}$ ) in the SLy4+HPA2 model is  $\sim 1.2M_{\odot}$ , so there is a huge gap  $\sim 0.7M_{\odot}$  between SLy4+HPA2 and KIDS0-Y4. The difference, being originated completely from the  $\Lambda$  hyperon interactions, makes sure the importance of higher order terms in the multiple density dependence of  $\Lambda$  hyperon energy functional.

KIDS-B, C, D models also show sharp changes of the MR curve at  $M \sim (1.8 - 1.9)M_{\odot}$ . Non-differentiability of the sharp peak is due to the existence of unstable ( $dP/d\rho < 0$ ) region. The instability can be removed by implementing Maxwell or Gibbs conditions. When the conditions are applied the MR curve will become smooth. KIDS0, and KIDS-B, C, D models have  $M_{\text{crit}}$  in the range  $(1.8 - 1.9)M_{\odot}$ . The result is interesting and important in the sense: i) Even though  $\rho_{\text{crit}}$  differs substantially among the KIDS model,  $M_{\text{crit}}$  is weakly dependent on them, ii) Multiple density dependence might be the major reason for the similarity of  $M_{\text{crit}}$ , iii) when the  $\Lambda$  interactions are determined in consistency with the nucleon model, a physical result  $M_{\text{crit}}$  becomes insensitive to the baseline nuclear model. The above points could be understood well if the behavior KIDS-D is compared to SLy4.  $\rho_{\text{crit}}$  of KIDS-D is  $3.2\rho_0$ , so it is much smaller than that of KIDS0,  $4.4\rho_0$ , but closer to that of SLy4  $2.8\rho_0$ . However,  $M_{\text{crit}}$  of the KIDS-D model differs from SLy4 by  $0.6M_{\odot}$ , but it is only  $0.1M_{\odot}$  smaller than the KIDS0 model.



Summarizing the result of the neutron star mass and radius, multiple density-dependent models give rise to  $M_{\text{crit}}$  weakly dependent on the symmetry energy. The  $M_{\text{crit}}$  from the KIDS model is  $(1.8 - 1.9)M_{\odot}$ , so EoS of canonical stars  $M = 1.4M_{\odot}$  is unlikely to be affected by the hyperon.

#### IV. SUMMARY AND CONCLUSION

The work was stimulated by the motivation i) Determine the in-medium interaction of  $\Lambda$  hyperon accurately, ii) Understand the effect of the uncertainty in the symmetry energy to the in-medium interaction of  $\Lambda$  hyperon.

In order to achieve the first goal, we employed the KIDS density functional formalism. Many-body contributions to the  $\Lambda$  hyperon interactions are expanded in the power of  $\rho^{1/3}$ , and parameters are determined by fitting to selected hypernuclear data. Improvement of fitting is examined by varying the number of density-dependent terms in the many-body interaction. Fitting becomes better with larger number of terms as expected, but the accuracy is increased in a stepwise form. With a single density dependence, fitting result is poor indeed, so even a few input data could not be reproduced. Accuracy of fitting is improved greatly when two or more density-dependent terms are considered.  $\chi^2$  values are similar for the 2- and 3-term fittings, and it reduces by a factor of about 2 with the 4 terms. Fitting with 5 terms gives only marginal improvement, so we concluded that fitting is sufficiently accurate with 4 density-dependent  $\Lambda$  hyperon many-body interactions. We confirmed that, with the 4 terms, all the data are reproduced within the error bars, and 5-term result is almost identical to that of the 4-term functional.

The second topic has been explored by using models consistent with nuclear properties and recent neutron star data, but have different symmetry energies. Parameters in the  $\Lambda$  hyperon interactions are fitted for each nuclear model with the number of density-dependent many-body interaction terms fixed to 4. We obtained similar values of  $\chi^2$  for all the models. The models are applied to the calculation of energy levels that are not included in the fitting. Single particles of heavy nuclei agree well with data at high orbital states such as  $f$  and  $g$  states, but the levels in the  $s$  state in light nuclei are consistently smaller than the experiment. Deviation from experiment for the light nuclei is 10 % or less in most cases.

In the next step, KIDS-Y4 models are applied to the calculation of the neutron star EoS.

Key results are summarized as i)  $\Lambda$  hyperons are not created at all, or start to be created at densities higher than  $3\rho_0$ , ii) Mass of the neutron star in which  $\Lambda$  hyperons exist is larger than  $1.8M_\odot$ , iii) Mass of the neutron star at which  $\Lambda$  hyperons start to exist is insensitive to the symmetry energy. Since hyperons contribute to the EoS at densities well above  $3\rho_0$  or in the stars heavier than  $1.8M_\odot$ , effect of the short range correlations could be non-negligible at these densities or masses. Therefore, a definitive conclusion about the hyperon puzzle might have to be postponed until the contributions of  $\Lambda\Lambda$  interactions, creation of other heavy baryons, pion or kaon condensations, and transition to quark matter phase are elaborated.

All in all, multiple density dependence in the nuclear energy density functional is not an optional choice, but a mandatory condition for an accurate and predictive description of the hypernuclei and the neutron star.

### Acknowledgments

The work of SC is supported by the Institute for Basic Science (IBS-R031-D1). The work of EH was supported by JSPS KAKENHI Grant Numbers JP18H05407 and JP20H00155. The work of CHH was supported by the National Research Foundation of Korea (NRF) grant funded by the Korea government (No. 2018R1A5A1025563 and No. 2020R1F1A1052495). The work of MKC was supported by the National Research Foundation of Korea (NRF) grant funded by the Korea government (No.2021R1A6A1A03043957 and No. 2020R1A2C3006177).

- 
- [1] T. O. Yamamoto *et al.*, Phys. Rev. Lett.**115**, 222501 (2015).
  - [2] O. Hashimoto, and H. Tamura, Prog. Part. Nucl. Phys. **57**, 564 (2006).
  - [3] A. Gal, J. M. Soper, and R. H. Dalitz, Ann. Phys. (NY), **63**, 53 (1971).
  - [4] D. J. Millener, A. Gal, C. B. Dover, and R. H. Dalitz, Phys. Rev. **C31**, 499 (1985).
  - [5] E. Hiyama and T. Yamada, Prog. Part. Nucl. Phys. **63**, 339 (2009).
  - [6] E. Hiyama, Few-body Sys. **53**, 189 (2012).
  - [7] M. M. Nagels *et al.*, Phys. Rev. **C99**, 044003(2019).
  - [8] F. Sakuma *et al.*, Taskforce on the extension of the Hadron Experimental Facility, "Extension of the J-PARC Hadron Experimental Facility", to be appeared in arXiv.

- [9] N. Guleria, S. Dhiman, and R. Shyam, Nucl. Phys. A **886**, 71 (2012).
- [10] H.-J. Schulze, and E. Hiyama, Phys. Rev. C **90**, 047301 (2014).
- [11] P. Papakonstantinou, T.-S. Park, Y. Lim, and C. H. Hyun, Phys. Rev. C **97**, 014312 (2018).
- [12] H. Gil, Y.-M. Kim, C. H. Hyun, P. Papakonstantinou, and Y. Oh, Phys. Rev. C **100**, 014312 (2019).
- [13] M. Ukai, *et al.*, Phys. Rev. Lett. **93**, 232501 (2004).
- [14] O. Hashimoto, *et al.*, Nucl. Phys. A **639**, 930 (1998).
- [15] T. Hasegawa, *et al.*, Phys. Rev. C **53**, 1210 (1996).
- [16] R. Bertini, *et al.*, Phys. Lett. B **83**, 306 (1979).
- [17] H. Tamura, *et al.*, Prog. Theor. Phys. **117**, 1 (1994).
- [18] R. E. Chrien, *et al.*, Nucl. Phys. A **478**, 705 (1988).
- [19] P. H. Pile, *et al.*, Phys. Rev. Lett. **66**, 2585 (1991).
- [20] H. Hotchi, *et al.*, Phys. Rev. C **64**, 044302 (2001).
- [21] H. Gil, and C. H. Hyun, New Physics: Sae Mulli **71**, 242 (2021).
- [22] Y. Lim, C. H. Hyun, K. Kwak, and C.-H. Lee, Int. J. Mod. Phys. E **24**, 1550100 (2015).
- [23] D. H. Davis, Nucl. Phys. A **754**, 3c (2005).
- [24] T. Hasegawa, *et al.*, Phys. Rev. Lett. **74**, 224 (1995).
- [25] Y. Miyura, *et al.*, Acta Phys. Polon. B **35**, 1019 (2004).
- [26] M Ahmed, *et al.*, Phys. Rev. C **68**, 064004 (2003).
- [27] S. Ajimura, *et al.*, Phys. Rev. Lett. **86**, 4255 (2001).
- [28] H. Kohri, *et al.*, Phys. Rev. C **65**, 034607 (2002).
- [29] F. Cusanno, *et al.*, Phys. Rev. Lett. **103**, 202501 (2009).
- [30] D. Gerstung, N. Kaiser, and W. Weise, Eur. Phys. J. A **56**, 175 (2020).
- [31] M. Kim, C.-H. Lee, Y.-M. Kim, K. Kwan, Y. Lim, and C. H. Hyun, Int. J. Mod. Phys. E **29**, 2030007 (2020).